Optics Letters

Sub-Hz relative linewidths from an interferometrically stabilized mid-infrared frequency comb

Dominic Laumer,[1,*] Sarper Salman,[1,2,3] Yuxuan Ma,[1] Kevin T. Zawilski,[4] Peter G. Schunemann,[4] Marcus Seidel,[1,2,3] Christoph M. Heyl,[1,2,3] and Ingmar Hartl[1]

[1]Deutsches Elektronen-Synchrotron DESY, Notkestr. 85, 22607 Hamburg, Germany
[2]Helmholtz-Institute Jena, Fröbelstieg 3, 07743 Jena, Germany
[3]GSI Helmholtzzentrum für Schwerionenforschung GmbH, Planckstraße 1, 64291 Darmstadt, Germany
[4]BAE Systems Inc., MER15-1813, P.O. Box 868, Nashua, New Hampshire 03061-0868, USA
*dominic.laumer@desy.de

Received 27 March 2023; revised 11 May 2023; accepted 13 May 2023; posted 15 May 2023; published 31 May 2023

Frequency combs present a unique tool for high-precision and rapid molecular spectroscopy. Difference frequency generation (DFG) of near-infrared sources is a common approach to generate passively stabilized mid-infrared combs. However, only little attention has been paid so far to precisely measure the coherence properties of such sources. Here, we investigate these using a Raman-soliton based DFG source driven by an Yb:fiber frequency comb. A heterodyne beat between the second harmonic of the phase-locked DFG comb near 4 μm and a 2 μm Tm:fiber frequency comb locked to the same optical reference is performed. Using this method, we measure the relative phase noise power spectral density of both combs. This results in a sub-Hz relative linewidth between the DFG comb and the Tm:fiber comb. We also introduce a new pump/seed delay locking mechanism based on interferometry for long-term stable intensity noise suppression.

https://doi.org/10.1364/OL.491684

Mid-infrared (MIR) optical frequency combs have become an important tool in science, industry, and health as the "molecular fingerprint" spectral region between 3 and 15 μm is filled with specific vibrational transitions in molecules. Frequency combs provide coherent light with orders of magnitude narrower linewidth and higher brightness compared with thermal light sources, enabling the detection of trace amounts of various molecules [1–5]. For vibrational spectroscopy, nonlinear frequency conversion is often used to downconvert the output of near-infrared (NIR) frequency combs into the MIR region. By employing $\chi^{(2)}$ nonlinearities, the NIR "pump" photons are split into "signal" and MIR "idler" photons [6,7]. This is done in optical parametric oscillators (OPOs) which can provide sub-Hz linewidths relative to the pump light [8–11]. However, OPOs require cavity length stabilization and excellent active control of the carrier-envelope-phase (CEP) to keep the intensity noise and the widths of the comb lines small. In contrast, difference frequency generation (DFG) or optical parametric amplification (OPA) sources come with passive carrier-envelope-offset stability [12] and do not require the synchronization of cavities. However, seed generation is neccessary to initiate the down-conversion process. Setups generating the pump radiation by blueshifting the driving laser were shown to be highly coherent down to Hz-level optical linewidths [13–15]. In other experiments, the seed was generated by coherently redshifting the pump laser, e.g., via Raman soliton self-frequency shifting or broadening in all-normal dispersion fibers [16,17]. However, comb linewidths of the generated DFG sources were not measured [18,19], showed linewidths in the 20–400 kHz range, or no coherent signal at all [20–23].

In this Letter, we characterize the coherence of a Raman-soliton based DFG frequency comb at 4 μm [18] by performing a heterodyne beat with a 2 μm Tm:fiber frequency comb locked to the same optical reference [24], measuring sub-Hz relative linewidths. Previously, we found that the relative intensity noise (RIN) of the MIR comb drops sharply in a small window around the perfect pump/seed temporal overlap. By implementing a dither locking scheme, we were able to reduce the RIN by approximately 30 dB and to increase the signal-to-noise ratio (SNR) in the measured spectra by a factor 1.7 compared to the free-running state [3,25]. However, dither-locking also generates sidebands to the comb lines. To circumvent this adverse effect, a different Δt locking mechanism based on interferometry is presented here. We show that with this method, sideband generation can be suppressed while the SNR of the measured spectra is slightly improved compared with the dither lock.

The MIR source is shown in the light-gray box of Fig. 1. It is based on an Yb:fiber laser frequency comb at $\lambda_{\mathrm{pump}} = 1060\,\mathrm{nm}$ with a repetition rate of $f_1 = 151.65\,\mathrm{MHz}$ and 1.5 W of average power. It is optically phase-locked by beating a comb line with a kHz-linewidth continuous wave Nd:YAG NPRO laser (Coherent Mephisto). The resulting radio frequency f_{Beat} as well as the carrier-envelope-offset frequency f_0, measured via self-referencing in an f–$2f$ interferometer, are stabilized by feedbacks to the cavity length and oscillator pump current/temperature, respectively. An additional feedback loop is used to correct drifts in the reference for f_1 stabilization as well by controlling its

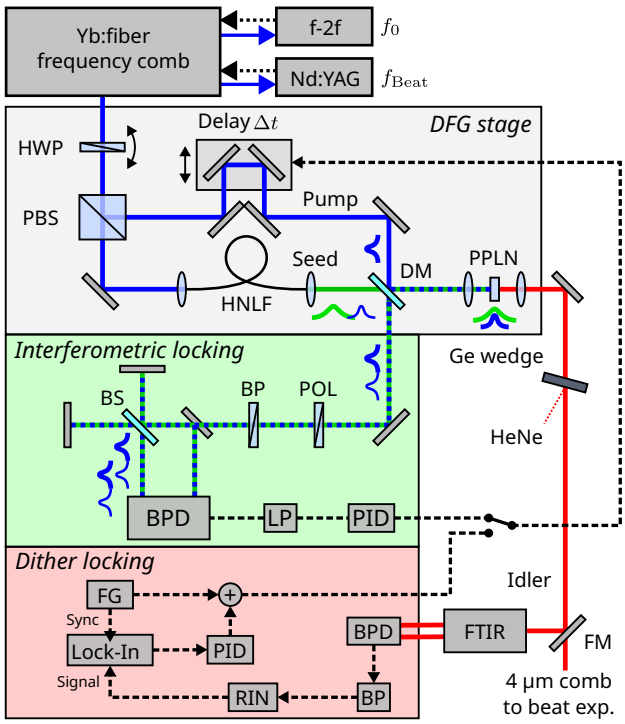

Fig. 1. Schematic overview of the experimental setup for the 4 µm frequency comb generation with both pump/seed delay locking schemes. HWP, half-wave plate; (P)BS, (polarizing) beam splitter; HNLF, highly nonlinear fiber; DM, dichroic mirror; PPLN, periodically poled lithium niobate; POL, polarizer; LP, lowpass filter; BP, bandpass filter; BPD, balanced photodiode; RIN, relative intensity noise detection; FG, function generator; PID, proportional-integral-derivative controller; FTIR, Fourier-transform spectrometer; FM, flip mirror.

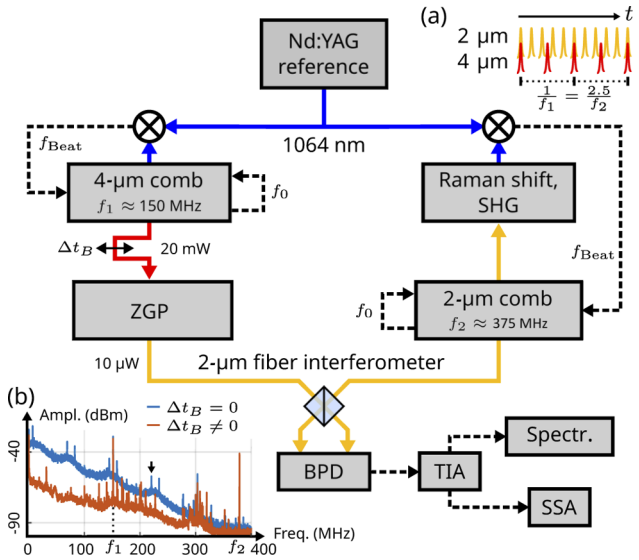

Fig. 2. Heterodyne beat setup for the linewidth measurement of the generated 4 µm frequency comb relative to a 2 µm Tm:fiber comb referenced to the same CW laser. ZGP, nonlinear crystal for SHG; TIA, transimpedance amplifier; SSA, signal source analyzer. (a) Temporal overlap occurs for every second pulse of the Yb-based comb and every fifth pulse of the Tm comb for repetition rates matching a ratio 2.5. (b) Measured beat note RF spectra both with (blue line) and without (red line) temporal overlap (Δt_B). The spectra were measured with 10 kHz resolution bandwidth (RBW). A small arrow denotes the beat note used for phase noise measurements.

cavity length and temperature. The laser output is split in pump and seed with the latter being coupled into a highly nonlinear suspended core fiber for tunable Raman soliton redshifting [26]. Its output is collinearly recombined with the pump using a dichroic mirror (DM), and focused into a periodically poled lithium niobate (PPLN) crystal for DFG. Temporal overlap Δt between pump and seed is achieved using a piezo-driven delay stage in the pump arm of the setup. The generated idler is collimated and separated from the pump and seed using a germanium wedge. The MIR beam is then either sent to a home-built FTIR spectrometer or a heterodyne beat setup. The wedge is also used to combine the beam with a red HeNe laser for alignment and FTIR calibration. For this work, the MIR source was set to 3.84 µm by means of the crystals poling period (29.09 µm), temperature (120°C), and Raman soliton wavelengths (1460 nm).

To characterize the coherence properties of the MIR comb, we beat its second harmonic (SHG) with a self-referenced Tm:fiber comb centered at 1.92 µm [27,28]. The setup is shown in Fig. 2. The Tm:fiber comb is also phase-locked to the kHz-linewidth NPRO reference. This is achieved by Raman-shifting the amplified Tm comb and subsequent frequency-doubling. Moreover, the repetition rate is adjusted to $f_2 = 2.5 \cdot f_1 = 379.125\,\mathrm{MHz}$ such that every fifth pulse is coinciding with every second pulse of the Yb-based comb. They are overlapped by a delay stage in the MIR beam path [Fig. 2(a)] and a fiber interferometer. The beat is detected with a home-built balanced photodiode (BPD) connected to a transimpedance amplifier using either an RF analyzer (Agilent E4402B) or a signal source analyzer (SSA, Agilent E5052B). In Fig. 2(b), we show the measured RF spectrum at $\Delta t_B \neq 0$, showing no beating, and at $\Delta t_B = 0$ with beat notes 10 dB above the noise floor.

While the active delay stabilization of the DFG scheme showed a clear MIR RIN reduction, its impact on the combs phase noise has not been studied. Here, we study this impact using the setup of Fig. 2 and compare measured beat notes with free-running, dither, and the new interferometric lock. For the dither lock (red box in Fig. 1), Δt is modulated using a small sinusoidal signal on the piezo stage. The MIR BPD of the FTIR measures its output continuously. The BPDs output is bandpass-filtered (1–30 kHz) and amplified by a demodulating logarithmic amplifier to determine a RIN-proportional signal. This signal is coupled into a lock-in amplifier (SRS SR530) generating an error signal for a proportional-integral-derivative (PID, SRS SIM960) controller, and the PIDs output is added to the input modulation to lock Δt to the RIN minimum. As Δt is modulated via a moving retro-reflector, we noticed that the setup is affected by the Doppler effect shifting the optical frequency of the pump by approximately 1 kHz per 0.5 mm/s of stage travel speed, close to the linewidth of the reference laser [29]. In addition, the sinusoidal movement gives rise to a phase modulation and subsequently to the generation of sidebands [Fig. 3(c)]. An analogous effect is targeted in electro-optical combs [30], but leads to an undesired distortion of the comb lines in our case. For this reason, a different delay locking scheme is implemented based on interference of residual 1060 nm light on the fourth port of the DM (green box in Fig. 1). This light is filtered in both

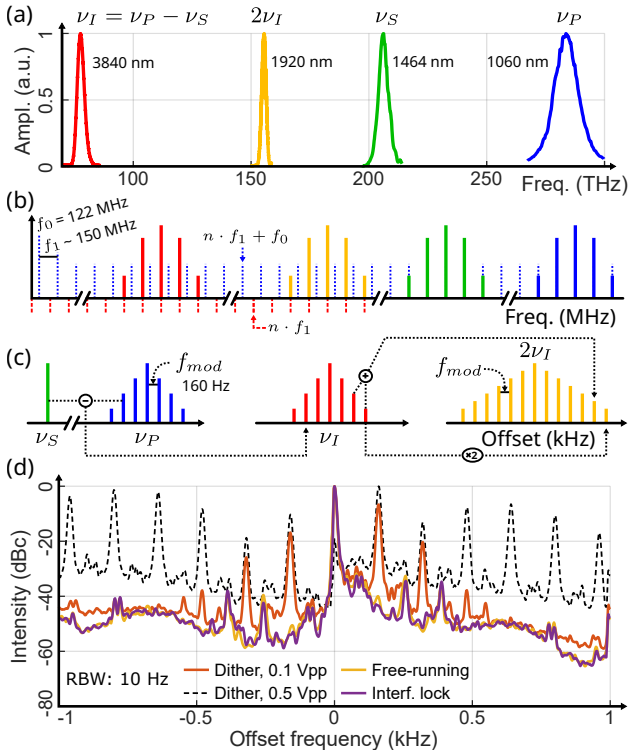

Fig. 3. Overview over the different spectral regimes of the Yb-based comb. (a) Measured normalized optical spectra in the THz range. (b) Comb structures for the optical fields, showing offset and spacing in the MHz regime. (c) Modulating the pump with Hz-level frequencies results in modulation of both the idler and its SHG. (d) Measured 2 μm beat notes with different pump/seed delay locking modes, showing significant sidebands for the two ditherings (red/blue, 160 Hz) and no changes between unlocked (yellow) and interferometrically locked (purple) states. Measured with 10 Hz RBW.

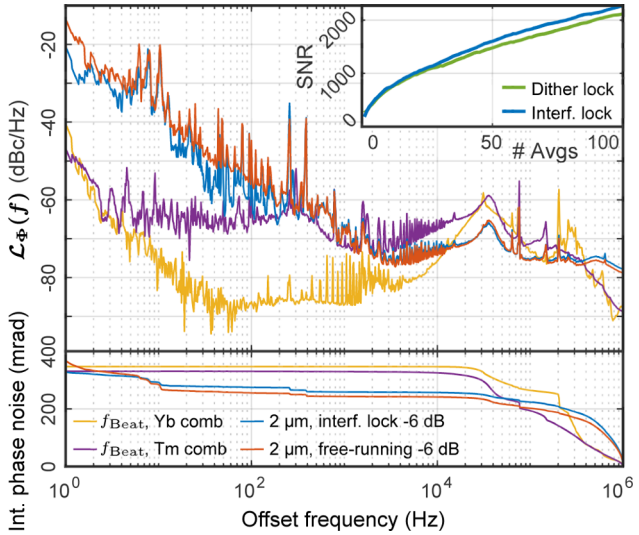

Fig. 4. Measured phase noises $\mathcal{L}_\Phi(f)$ of the beat note (−6 dB) between the Tm comb and frequency-doubled MIR comb with (blue line) and without (red line) interferometric stabilization. Furthermore, the phase noises of the beats between the NPRO reference and the Yb comb (yellow line) and Tm comb (violet line) are shown. The inset shows the SNR of the MIR spectra measured with a home-built FTIR spectrometer increasing with the number of integrated spectra. Both the dither mechanism and the presented interferometric locking were used, showing a slightly better SNR with the new method.

spectrum and polarization, and coupled into a Michelson interferometer to counteract the group delay caused by the HNLFs dispersion difference between 1060 nm and the redshifted soliton. This ensures temporal overlap for both wavelengths and is visualized with small pulse symbols along the beam paths. The interferometer is setup such that the backreflection can be picked up with a mirror and used for balanced detection, reducing the influence of intensity fluctuations on the measured interference. The signal is then fed into a PID to drive the stage toward the interference fringe center with a locking bandwidth of approximately 250 Hz, residual optical path difference fluctuations of less than 10 nm ($\lambda_{pump}/100$) rms.

To elaborate further on the coherence properties of the Yb-based comb, we show its spectrum on three different frequency scales in Fig. 3. In Fig. 3(a), the measured optical spectra in the 100s of THz range are shown. In Fig. 3(b), the frequency comb structures for input and output fields are visualized schematically. The Yb-based comb lines are multiples of the repetition rate $f_1 \approx 150$ MHz with pump and seed being offset by $f_0 = 122$ MHz. The dither lock generates sidebands to the pump comb lines. As Fig. 3(c) explains, these are transferred to the frequency-doubled MIR comb and thus observed in the heterodyning experiment. Figure 3(d) compares beat note measurements near 6.9 MHz without jitter compensation to those applying interferometric locking or a sinusoidal modulation as used in the dither lock. This data was taken with the RF spectrometer. For the dithering, we also show two different modulation amplitudes (0.1 V and 0.5 V) with the modulation frequency $f_{mod} = 160$ Hz, resulting in increased sideband generation at higher voltage. In all cases, the measured linewidth for the central beat note is limited by the spectrometer's resolution of 10 Hz. As expected, the dithering introduces clearly visible sidebands with f_{mod} spacing. For the stabilization of the MIR comb, peak voltages of 0.1 V are typical. These induce sidebands which are visible within a ±0.5 kHz span around the central beat frequency. In contrast, we do not observe differences between the beat notes with interferometric and without locking. We note that the stabilization is not primarily expected to reduce the linewidth but to significantly decrease the RIN of the MIR comb [25].

Eventually, we characterized the phase noise $\mathcal{L}_\Phi(f)$ of the beat notes with the SSA [31]. For these measurements, we filter out the beat note at 221 MHz [shown in Fig. 2(b) with a small arrow] using a tunable bandpass filter. The results are shown together with the phase noise measurements of the beats with the NPRO reference for both Yb and Tm combs in Fig. 4. These show similar performance with an integrated phase noise (1 MHz to 1 Hz) of 330 mrad and 347 mrad for the Tm laser and the Yb laser, respectively. For the 2 μm signals, we subtract 6 dB to get the phase noise for the fundamental MIR comb before the SHG [32], halving the integrated phase noise. Above offset frequencies of 1 kHz, the data shows good agreement in the noise spikes between the comb's heterodyne signal and the f_{Beat} locks. Below 1 kHz , acoustic noise dominates the phase noise with significant peaks at 258 Hz and 388 Hz, most likely caused by mechanical resonances of the pump/seed delay stage. The

integrated phase noise (1 MHz to 1 Hz) is 328 mrad for the interferometric lock and 368 mrad for the free-running state. Following [33], this translates to a sub-Hz linewidth for the 4 μm MIR comb relative to the reference. As the setup was built for high-resolution absorption spectroscopy, we also measure the spectral quality of the MIR beam in a home-built FTIR spectrometer. Previously, a significant increase in spectral SNR was demonstrated when the free-running comb was locked by the dither method [25]. Here, we use the same approach to directly compare the spectral SNR of the comb locked by the dither and the interferometric method. We collect 200 spectra for both locks over an hour and average two subsets consisting of increasing numbers of spectra. The two subsets are then divided and the ratio's inverse standard deviation within the spectra's FWHM is calculated. The resulting number is a figure-of-merit for the SNR of features with 100% absorption. It is shown in the small inset in Fig. 4. These data prove the long-term stability of the interferometric lock by showing a slight improvement over the dither-lock after averaging over the full data set.

In conclusion, we have directly measured the optical linewidth of our DFG-based frequency comb relative to a 2 μm Tm:fiber comb using the same kHz-linewidth reference laser. Using the heterodyning setup, we were able to compare two different schemes to stabilize the relative delay between pump and seed beams to $\Delta t = 0$. By dithering, we measured a significant generation of sidebands at the dithering frequency which effectively reduce the resolution in MIR comb spectroscopy. Compared with this, the new interferometric lock shows no discernible difference to the free-running state on a short time scale. Furthermore, the phase noise measurements of the beat notes yields a sub-Hz linewidth of the generated MIR comb relative to the reference laser. In addition to this, the new method is also tested in a comb spectroscopy setup with our home-built FTIR and was proven to enable long-term operation as well. The interferometric locking thus enables both high-resolution and high-sensitivity MIR frequency comb spectroscopy. As such, the system would be able to provide insights into e.g., molecular parity violations [34] or nuclear-spin-forbidden rovibrational transitions in water [35]. Beyond that, the method can be generalized to other cases where temporal overlap between two at least partially interfering beams is critical.

Funding. Helmholtz Association; Deutsches Elektronen-Synchrotron.

Disclosures. The authors declare no conflicts of interest.

Data availability. Data underlying the results presented in this Letter are not publicly available at this time but may be obtained from the authors upon reasonable request.

REFERENCES

1. A. Schliesser, N. Picqué, and T. W. Hänsch, Nat. Photonics **6**, 440 (2012).
2. K. C. Cossel, E. M. Waxman, I. A. Finneran, G. A. Blake, J. Ye, and N. R. Newbury, J. Opt. Soc. Am. B **34**, 104 (2017).
3. G. Yang, V. S. de Oliveira, D. Laumer, C. M. Heyl, A. Yachmenev, I. Hartl, and J. Küpper, J. Mol. Spectrosc. **392**, 111744 (2023).
4. A. Foltynowicz, P. Masłowski, A. J. Fleisher, B. J. Bjork, and J. Ye, Appl. Phys. B **110**, 163 (2013).
5. Q. Liang, Y.-C. Chan, P. B. Changala, D. J. Nesbitt, J. Ye, and J. Toscano, Proc. Natl. Acad. Sci. **118**, e2105063118 (2021).
6. V. Petrov, Prog. Quantum Electron. **42**, 1 (2015).
7. K. Tian, L. He, X. Yang, and H. Liang, Photonics **8**, 290 (2021).
8. F. Adler, K. C. Cossel, M. J. Thorpe, I. Hartl, M. E. Fermann, and J. Ye, Opt. Lett. **34**, 1330 (2009).
9. N. Leindecker, A. Marandi, R. L. Byer, and K. L. Vodopyanov, Opt. Express **19**, 6296 (2011).
10. A. Marandi, N. C. Leindecker, V. Pervak, R. L. Byer, and K. L. Vodopyanov, Opt. Express **20**, 7255 (2012).
11. K. F. Lee, C. Mohr, J. Jiang, P. G. Schunemann, K. L. Vodopyanov, and M. E. Fermann, Opt. Express **23**, 26596 (2015).
12. M. Zimmermann, C. Gohle, R. Holzwarth, T. Udem, and T. W. Hänsch, Opt. Lett. **29**, 310 (2004).
13. F. C. Cruz, D. L. Maser, T. Johnson, G. Ycas, A. Klose, F. R. Giorgetta, I. Coddington, and S. A. Diddams, Opt. Express **23**, 26814 (2015).
14. D. L. Maser, G. Ycas, W. I. Depetri, F. C. Cruz, and S. A. Diddams, Appl. Phys. B **123**, 142 (2017).
15. C. Cleft, M. Bradler, P. Adel, S. Matern, M. Fischer, and R. Holzwarth, in *Conference on Lasers and Electro-Optics* (Optica Publishing Group, 2020), p. SF2G.1.
16. A. Ruehl, M. J. Martin, K. C. Cossel, L. Chen, H. McKay, B. Thomas, C. Benko, L. Dong, J. M. Dudley, M. E. Fermann, I. Hartl, and J. Ye, Phys. Rev. A **84**, 011806 (2011).
17. A. M. Heidt, A. Hartung, G. W. Bosman, P. Krok, E. G. Rohwer, H. Schwoerer, and H. Bartelt, Opt. Express **19**, 3775 (2011).
18. A. Ruehl, A. Gambetta, I. Hartl, M. E. Fermann, K. S. E. Eikema, and M. Marangoni, Opt. Lett. **37**, 2232 (2012).
19. M. Seidel, X. Xiao, S. A. Hussain, G. Arisholm, A. Hartung, K. T. Zawilski, P. G. Schunemann, F. Habel, M. Trubetskov, V. Pervak, O. Pronin, and F. Krausz, Sci. Adv. **4**, eaaq1526 (2018).
20. T. W. Neely, T. A. Johnson, and S. A. Diddams, Opt. Lett. **36**, 4020 (2011).
21. L. Jin, V. Sonnenschein, M. Yamanaka, H. Tomita, T. Iguchi, A. Sato, K. Nozawa, K. Yoshida, S.-I. Ninomiya, and N. Nishizawa, IEEE J. Sel. Top. Quantum Electron. **24**, 1 (2018).
22. G. Soboń, T. Martynkien, P. Mergo, L. Rutkowski, and A. Foltynowicz, Opt. Lett. **42**, 1748 (2017).
23. A. Gambetta, M. Cassinerio, N. Coluccelli, E. Fasci, A. Castrillo, L. Gianfrani, D. Gatti, M. Marangoni, P. Laporta, and G. Galzerano, Opt. Lett. **40**, 304 (2015).
24. W. Swann, J. McFerran, I. Coddington, N. Newbury, I. Hartl, M. Fermann, P. Westbrook, J. Nicholson, K. Feder, C. Langrock, and M. Fejer, Opt. Lett. **31**, 3046 (2006).
25. V. S. de Oliveira, A. Ruehl, P. Masłowski, and I. Hartl, Opt. Lett. **45**, 1914 (2020).
26. L. Dong, B. K. Thomas, and L. Fu, Opt. Express **16**, 16423 (2008).
27. C.-C. Lee, C. Mohr, J. Bethge, S. Suzuki, M. E. Fermann, I. Hartl, and T. R. Schibli, Opt. Lett. **37**, 3084 (2012).
28. J. Jiang, C. Mohr, J. Bethge, A. Mills, W. Mefford, I. Hartl, M. E. Fermann, C.-C. Lee, S. Suzuki, T. R. Schibli, N. Leindecker, K. L. Vodopyanov, and P. G. Schunemann, *Conference on Lasers and Electro-Optics 2012* (Optical Society of America, 2012), p. CTh5D.7.
29. H. E. Ives, J. Opt. Soc. Am. **30**, 255 (1940).
30. A. Parriaux, K. Hammani, and G. Millot, Adv. Opt. Photonics **12**, 223 (2020).
31. R. Scott, C. Langrock, and B. Kolner, IEEE J. Sel. Top. Quantum Electron. **7**, 641 (2001).
32. M. Delehaye, J. Millo, P.-Y. Bourgeois, L. Groult, R. Boudot, E. Rubiola, E. Bigler, Y. Kersalé, and C. Lacroûte, IEEE Photonics Technol. Lett. **29**, 1639 (2017).
33. J. Hall and M. Zhu, *An Introduction to Phase-Stable Optical Sources* (North-Holland, 1993), Vol. CXVIII. JILA Pub. 4738.
34. M. R. Fiechter, P. A. B. Haase, N. Saleh, P. Soulard, B. Tremblay, R. W. A. Havenith, R. G. E. Timmermans, P. Schwerdtfeger, J. Crassous, B. Darquié, L. F. Pašteka, and A. Borschevsky, J. Phys. Chem. Lett. **13**, 10011 (2022).
35. A. Yachmenev, G. Yang, E. Zak, S. Yurchenko, and J. Küpper, J. Chem. Phys. **156**, 204307 (2022).